# RF Power Performance of Sc(Al,Ga)N/GaN HEMTs at Ka-Band

Andrew J. Green, *Member*, Neil Moser, Nick Miller, Kyle J. Liddy, Miles Lindquist, Michael Elliot, *IEEE*, James K. Gillespie, Robert C. Fitch, Jr., *Sr. Member*, Ryan Gilbert, *IEEE*, Dennis E. Walker, Jr., *Member, IEEE*, Elizabeth Werner, *Member, IEEE*, Antonio Crespo, Edward Beam, *Member, IEEE* , Andy Xie, Cathy Lee, Yu Cao, *Sr. Member, IEEE*, and Kelson D. Chabak, *Member, IEEE*

***Abstract*—We report the RF power results of Sc(Al,Ga)N/GaN high electron mobility transistors (HEMTs). We show dc, small-signal RF and load-pull performance at 30 GHz with two barrier alloys—a ternary of ScAlN and a quaternary of ScAlGaN. The active layers are grown by molecular beam epitaxy on a GaN-on-SiC template. The Sc(Al,Ga)N HEMTs with 120 nm gate length achieve transconductance > 700 mS/mm and > 70 GHz cutoff frequency. The quaternary ScAlGaN sample shows reduced current collapse during pulsed I-V and load-pull characterization. The ScAlGaN HEMT delivers 5.77 W/mm output power ($V_D$= 20 V) and 47% power-added efficiency ($V_D$= 15 V) when tuned for maximum power and efficiency, respectively.**

***Index Terms*—ScAlN, ScAlGaN, GaN, radio frequency, dispersion, small-signal, large-signal, HEMT**

## I. Introduction

Next-generation GaN-based amplifiers require low sheet resistance and a thin barrier layer to meet efficient radio frequency (RF) power demands for millimeter-wave applications. Multiple approaches have accomplished this by adjusting the barrier alloy to increase the total polarization charge in the GaN channel with varying levels of piezoelectric charge such as in strained InAlN/GaN [1]–[3], AlN/GaN HEMTs[4]–[6] as well as N-polar variations[7][8][9]. Lattice-matched $In_{0.18}Al_{0.72}N$/GaN HEMTs have been reported with performance in X and Ka-band but with limits on spontaneous induced sheet charge[10]–[12].

Attributed to the spontaneous polarization coefficient ScAlN [13][14][15], ScAlN/GaN can also be lattice-matched with up to 2x sheet charge density compared to $In_{0.18}Al_{0.72}N$/GaN [15][16]. It has been shown that lattice-mismatch causes defect generation leading to device degradation in Al and In based alloys [17][18]. A lattice-matched Sc-based barrier enables high sheet charge density without strain and may enhance reliability.

Currently the whitespace for high current/high power applications is being evaluated with respect to these tradeoffs. Sc(Al,Ga)N growths have been reported by molecular beam epitaxy (MBE) [15], [19], and a ScAlN/GaN HEMT was recently reported with impressive dc and small-signal RF performance [20].

Here, we report RF power performance of Sc(Al,Ga)N/GaN HEMTs. Two samples were grown by MBE with a ternary ScAlN and quaternary ScAlGaN barrier to compare the tradeoff in sheet charge density with respect to mobility as Ga is introduced. These devices have improved short-channel effects over previously reported ScAlN/GaN HEMTs [20]. State-of-the-art DC performance is reported for each while pulsed *I-V* and 30-GHz power sweeps indicate differences in current collapse between the two samples. Both samples achieve > 10 dB transducer gain ($G_T$) at 30 GHz. The quaternary ScAlGaN/GaN HEMT achieved 5.77 W/mm output power ($P_{OUT}$) and 47% power-added efficiency (PAE) when tuned for optimal $P_{OUT}$ and PAE, respectively. The early RF power performance nearly matches state-of-the-art Ga-polar devices at our reported frequency and bias conditions [9][21][22][23][24].

## II. Epitaxial Growth and Device Fabrication

Epitaxial structure design and growth were performed by Qorvo. A nucleation, GaN buffer and GaN channel layer was grown by MOCVD followed by a 1 and 2 nm spacer layer of AlN and $Al_{0.25}Ga_{0.75}N$, respectively. The wafer was then immediately loaded into a gas source MBE reactor, followed by the growth of lattice matched 5.5 nm of $Sc_{0.18}Al_{0.72}N$ or 5.3 nm $Sc_{0.07}Al_{0.38}Ga_{0.55}N$ barrier layers, nominally. The growth of quaternary is achieved by adding Ga flux into ScAlN growth without adjusting other growth parameters. The exact compositions are still subject of research due to the lack of reliable material data such as lattice constants, etc. Finally, 1.2 nm of a GaN capping layer was grown.

Nominal layer thicknesses and material properties area shown in Table 1. The Hall data was obtained from separate calibration samples grown on sapphire substrates without surface passivation. An expected decrease in the sheet charge density is observed as Sc is replaced with Ga.

Sc(Al,Ga)N/GaN HEMTs were fabricated with regrown ohmic contacts using the same process from reference [20]. Devices reported in this manuscript have a $4\times65\,\mu$m total gate

Manuscript received April 4, 2019; accepted May 2, 2019. Date of publication May 8, 2019; date of current version June 26, 2019. This work was supported by the Air Force Research Laboratory (AFRL).

(Corresponding author: Andrew J. Green.) A. J. Green, N. Moser, N. Miller, K. Liddy, J. K. Gillespie, R. C. Fitch, Jr., D. E. Walker, Jr., A. Crespo, and K. D. Chabak, are with Wright-Patterson Air Force Base, Air Force Research Laboratory (AFRL), Dayton, OH 45433 USA (e-mail: andrew.green.25@us.af.mil). M. Lindquist, M. Elliot, R. Gilbert and E. Werner is with KBRwyle, Dayton, OH 45433 USA.

E. Beam, A. Xie, C. Lee, and Y. Cao are with Qorvo, Richardson, TX 75082 USA. Digital Object Identifier 10.1109/LED.2019.2915555

**Table 1: Sample Material Properties**

| | Gate-to-channel distance (nm) | Ra (nm) | $R_{SH}$ (Ω/□) | $n_s$ ($cm^{-2}$) | Mobility ($cm^2/V·s$) |
|---|---|---|---|---|---|
| ScAlN/GaN | ~9.7 | 0.21 | 233 | 2.4e13 | 1110 |
| ScAlGaN/GaN | ~9.5 | 0.32 | 259 | 1.76e13 | 1370 |

periphery with source connected electroplated air bridges. The HEMT channels were protected by $SiO_2$ deposited by plasma-enhanced chemical vapor deposition (PECVD) during ohmic contact regrowth. The devices have a 200 nm PECVD silicon-rich SiN surface passivation which has suppressed current collapse in multiple barrier designs [3][11][12][25]. Ni/Au T-shaped gates with 120 ± 20 nm gate length ($L_G$) were defined by electron beam lithography with an offset of 0.5 $\mu$m towards the source electrode from the center of the channel. The source-to-drain distance ($L_{SD}$) is 3 $\mu$m. Contact resistance ($R_C$) for the devices was extracted from transmission line measurement (TLM) test structures as < 0.1 Ωmm for both samples.

## III. DC AND PULSED PERFORMANCE

Representative dc *I-V* performance is shown in Fig. 1 for each sample with the device dimensions described in Sec II. Fig. 1(a) shows the family of output curves for the ScAlN/GaN (black) and ScAlGaN/GaN (blue) HEMTs. The ScAlN/GaN (ScAlGaN/GaN) devices have low on-resistance ($R_{ON}$) and high maximum current density ($I_{DS,max}$) of 1.01 (0.89) Ω·mm, and 1.92 (1.73) A/mm, respectively. Fig. 1(b) shows the log($I_{DS}$) and transconductance ($G_m$) transfer characteristics with a peak $G_m$= 700 (701) mS/mm measured at $V_{DS}$= 10 V. The on/off current ratio is ~$10^4$ ($10^3$) and is mainly limited by high Schottky gate off-state leakage which remains under investigation.

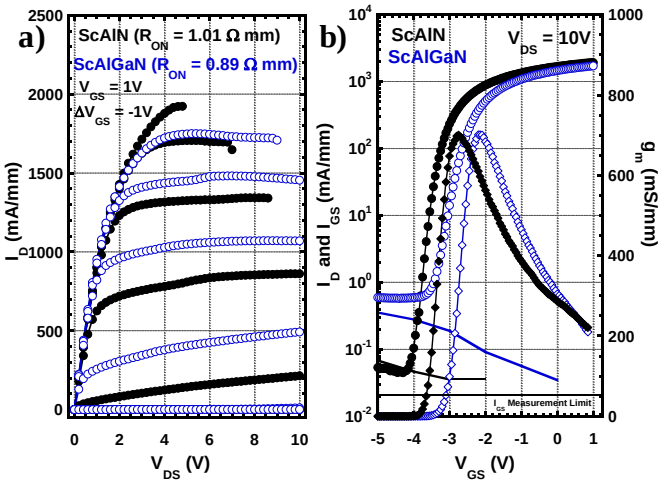


**Fig. 1. Representative a) output $I_{DS}$ vs. $V_{DS}$ family of curves and b) transfer characteristics for a 4x65 $\mu$m HEMT from each sample.**

The negative threshold voltage ($V_{TH}$) shift for the ScAlN/GaN sample can be attributed to the higher sheet charge density according to Table 1. While not shown, a soft breakdown voltage ($V_{BK}$) limited by gate leakage is recorded at 15.8 (16.0) V defined by current compliance at 2 mA/mm in the off-state. Hard $V_{BK}$ is expected to be >40V due to successful repeated power sweeps at $V_D$ = 20V. Improved device performance is expected by eliminating gate leakage and optimizing the gate-to-drain distance without affecting the breakdown voltage [26].

Fig. 2 shows pulsed *I-V* performance for each sample type. In Figs. 2(a-b), pulses with 400 ns width and 5 ms period were applied to the gate and drain quiescent voltage ($V_{Gq}$, $V_{Dq}$) points (0V,0V), (-6V,0V) and (-6V,10V). The filled data points show the effect of both gate and drain lag. The magnitude of current collapse is defined as the ratio of $I_{DS}$ at the (0V,0V) and (-6V,10V) conditions taken at the knee voltage ($V_K$) for the (0V,0V) curve. Significant dispersion is observed on the ScAlN/GaN sample compared to the ScAlGaN/GaN, but the origin of this current collapse is not yet understood. Figs. 2(c-d) show wafer scale heat maps (9 row x 10 columns, ~900 $mm^2$) of the total lag ratio (*TLR*) indicating uniform 59.7% ± 9.2% and just 6.5% ± 0.8% on the ScAlN/GaN and ScAlGaN/GaN samples, respectively. We note that the GaN cap likely does not play a strong role in suppressing charge trapping since a third ScAlGaN wafer without a GaN cap was fabricated and showed total current collapse of 5% ± 3%.

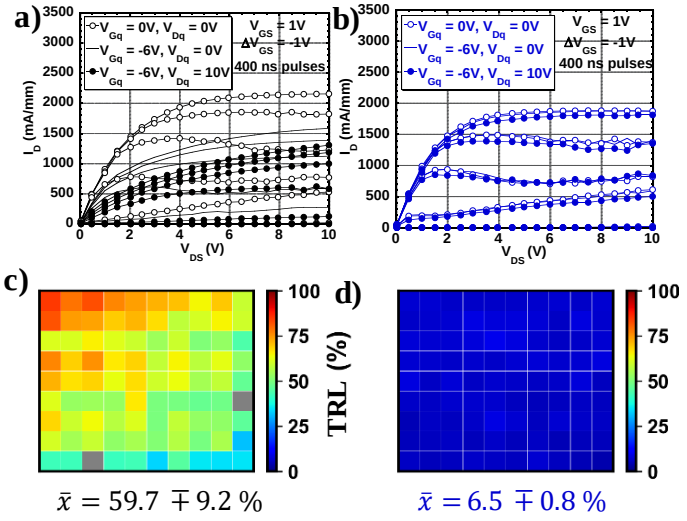


**Figure 2. 400-ns (5 ms period) pulsed *I-V* performance with three quiescent points for the (a) ScAlN/GaN and (b) ScAlGaN/GaN HEMTs. A 9 row x 10 column heat map (~900 $mm^2$) of the total gate and drain lag (TLR%) is shown for the (c) ScAlN/GaN and (d) ScAlGaN/GaN HEMT wafers.**

Current collapse can be caused by many factors such as the alloy composition, growth condition, chamber history, and passivation. It originates from the depletion of 2DEG in the channel by trapped electrons located at the epitaxial surface or in the layers above the channel. It has been reported previously that current collapse may increase with reduced distance between the 2DEG location and the surface per the charge/distance relationship in Columbic force equation [27].

To understand the difference of the current collapse in HEMTs with ternary and quaternary barriers, we applied the Fang-Howard model [28] to calculate the 2DEG centroid position by $< z > \int_0^\infty z|\varphi(z)|^2 dz$, where the AlN/GaN interface is defined at z=0 and the wave function $\varphi(z)$ is given by $\varphi(z) = \sqrt{\frac{b^3}{2}} z e^{-bz/2}$ where $b = (33m * q^2 n_s / 8\hbar^2 \varepsilon_0 \varepsilon_{GaN})^{1/3}$, m* is the effective mass of electron in GaN, q

is the electron charge, ħ is the reduced Planck's constant, $\varepsilon_0$ is the permittivity of vacuum and $\varepsilon_{GaN}$ is the dielectric constant of GaN. Assuming all gate voltage drops across the Sc(Al,Ga)N/AlGaN/AlN layers, we calculate the charge density change in the channel as a function of gate bias.

As expected, the centroid position moves farther away from the AlGaN/Sc(Al,Ga)N regrown interface with increasingly negative gate bias. The distance between the gate and centroid position is shown in Fig. 3. This indicates under the same $V_G$, the 2DEG in the ScAlGaN HEMT is less depleted from the trapped charges located above the interlayer—those either at the epitaxial surface or AlGaN/Sc(Al,Ga)N regrown interface resulting in less current collapse.

Since the pinch-off voltage does not change in both HEMTs in the pulsed I-V measurements, the traps most likely remain in the access region between the gate and drain/source instead of under the gate. This can be observed from the larger dispersion measured at the (-6V,0V) Q point. Further investigation is required to determine if these traps are located at the Sc(Al,Ga)N/AlGaN interface or in the Sc(Al,Ga)N layer. Higher current collapse in ScAlN could also be attributed to more trapping states in the ternary alloy compared to the quaternary.

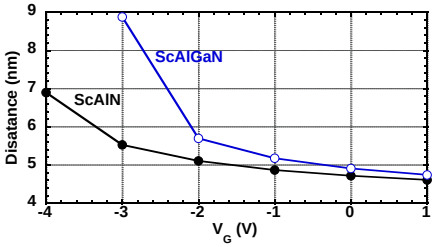


**Fig. 3. Distance between the 2DEG centroid and AlGaN/ScAl(Ga)N regrown interface as a function of $V_G$.**

## IV. Small and Large Signal RF Performance

Small signal RF performance of the devices is shown for both wafers in Fig. 4. S-paramaters were measured from 0.1 – 40 GHz at $V_{DS}$= 10V and $V_{GS}$ corresponding to 10% $I_{DSS}$ ($I_{DS}$ measured at $V_{GS}$= 0V) which is relevant for class-AB power conditions. The devices from each sample performed nearly identically with a current gain cutoff frquency ($f_T$) and maximum oscillating frequency ($f_{MAX}$) of about $f_T/f_{MAX}$= 72/102 GHz using a -20 dB/dec extrapolation.

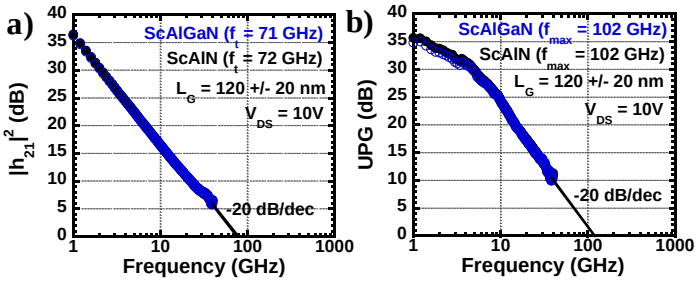


**Fig. 4.a) Current gain and b) unilateral power gain versus frequency for each sample with the extrapolated $f_T$ and $f_{MAX}$ indicated at $V_{DS}$= 10V and $V_{GS}$ corresponding to 39.5 (37.0) mA.**

Ka-band power performance of the Sc(Al,Ga)N/GaN HEMTs was evaluated using class-AB power sweeps at 30 GHz configured. In Fig. 5(a) each device was driven with input power ($P_{IN,AV}$) until $G_T$ compresses by 3 dB at $V_{DS}$= 15V while tuned for maximum $G_T$. The $G_T$ compresses at ~7 dB higher $P_{IN,AV}$ for the ScAlGaN/GaN sample which is attributed to differences in current collapse shown in Fig. 2. The ternary (quaternary) measures a maximum $P_{OUT}$ of 0.89 (3.55) W/mm and a PAE of 16.0 (31.0)% at $V_G$=-2.94 (-2.65) V. Fig. 5(b) shows the highest performance achieved during the power sweep. When impedance matched for efficiency, the quaternary device was able to achieve 47% PAE with the drain biased at $V_D$= 15V with a $P_{OUT}$ of 3.54 W/mm. The same device was then tested at $V_D$= 20V while tuned for $G_T$ and reached a maximum $P_{OUT}$ of 5.77 W/mm with a PAE of 43%. The reported RF power performance is near state-of-the-art when benchmarked with Ga-polar 30-GHz RF power performance reviewed in ref [9].

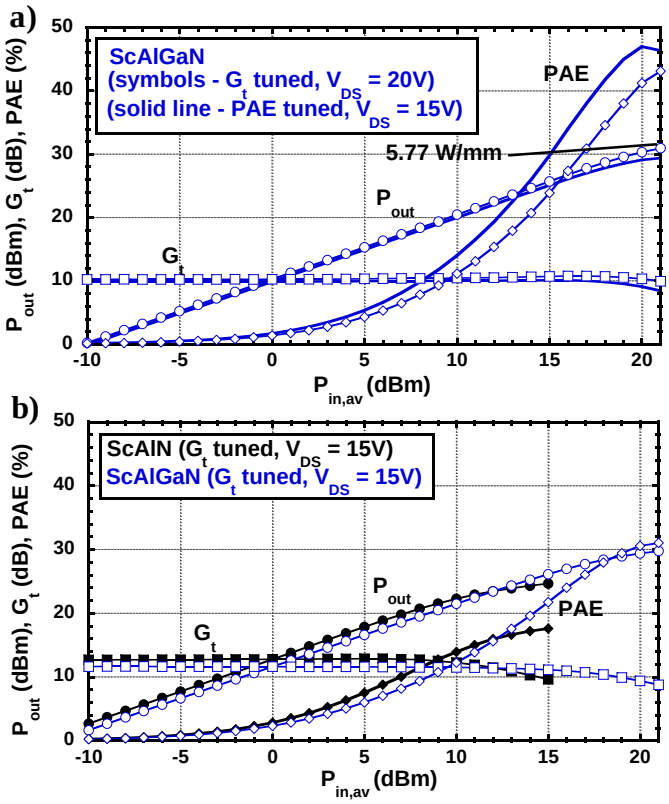


**Fig 5. Load Pull at 30 GHz for the devices in Figure 1 at (top) $V_{DS}$ =15 V with optimal $G_t$ tuning and (bottom) the best RF performance reported for each sample up to $V_{DS}$= 20 V with tuning conditions indicated.**

## V. Conclusions

RF power performance was compared between a ScAlN/GaN and ScAlGaN/GaN sample with varying sheet charge density and mobility characteristics. Both samples achieve high $G_M$ and $f_{MAX}$ around 700 mS/mm and 102 GHz, respectively. The ScAlN sample had higher current collapse which is theorized to originate from the difference in the 2DEG centroid position with respect to the barrier layer. The ScAlGaN/GaN wafer delivered 5.77 W/mm $P_{OUT}$ ($V_D$= 20V) and 47.0% efficiency ($V_D$= 15V) with optimal tuning. Both sample types are expected to significantly improve with materials maturation and device research to suppress gate leakage and traps that limit the power performance presented in this manuscript.

## REFERENCES


[1] R. Wang, G. Li, J. Verma, B. Sensale-Rodriguez, T. Fang, *et al.*, "220-GHz quaternary barrier InAlGaN/AlN/GaN HEMTs," *IEEE Electron Device Lett.*, vol. 32, no. 9, pp. 1215–1217, 2011, doi: 10.1109/LED.2011.2158288.

[2] A. Crespo, M. Bellott, K. Chabak, J. K. Gillespie, G. H. Jessen, *et al.*, "High frequency performance of Ga free barrier AlInN/GaN HEMT," *Phys. Status Solidi Curr. Top. Solid State Phys.*, vol. 7, no. 10, pp. 2433–2435, 2010, doi: 10.1002/pssc.200983886.

[3] K. D. Chabak, M. Trejo, A. Crespo, D. E. Walker, J. Yang, *et al.*, "Strained AlInN/GaN HEMTs on SiC with 2.1-A/mm output current and 104-GHz cutoff frequency," *IEEE Electron Device Lett.*, vol. 31, no. 6, pp. 561–563, 2010, doi: 10.1109/LED.2010.2045099.

[4] D. F. Brown, K. Shinohara, A. L. Corrion, R. Chu, A. Williams, *et al.*, "High-speed, enhancement-mode GaN power switch with regrown n+ GaN ohmic contacts and staircase field plates," *IEEE Electron Device Lett.*, vol. 34, no. 9, pp. 1118–1120, 2013, doi: 10.1109/LED.2013.2273172.

[5] K. Shinohara, D. C. Regan, Y. Tang, A. L. Corrion, D. F. Brown, *et al.*, "Scaling of gan hemts and schottky diodes for submillimeter-wave mmic applications," *IEEE Trans. Electron Devices*, vol. 60, no. 10, pp. 2982–2996, 2013, doi: 10.1109/TED.2013.2268160.

[6] Y. Tang, K. Shinohara, D. Regan, A. Corrion, D. Brown, *et al.*, "Ultrahigh-Speed GaN High-Electron-Mobility Transistors With $f_T/f_{max}$ of 454 / 444 GHz," *IEEE Electron Device Lett.*, vol. 36, no. 6, pp. 549–551, 2015.

[7] B. Romanczyk, M. Guidry, S. Wienecke, H. Li, E. Ahmadi, *et al.*, "W-Band N-Polar GaN MISHEMTs with High Power and Record 27.8% Efficiency at 94 GHz," in *2016 IEEE INTERNATIONAL ELECTRON DEVICES MEETING (IEDM)*, 2016.

[8] S. Wienecke, B. Romanczyk, M. Guidry, H. Li, E. Ahmadi, *et al.*, "N-polar gaN cap MISHEMT with Record Power Density Exceeding 6.5 W/mm at 94 GHz," *IEEE Electron Device Lett.*, vol. 38, no. 3, pp. 359–362, 2017, doi: 10.1109/LED.2017.2653192.

[9] B. Romanczyk, S. Wienecke, M. Guidry, H. Li, E. Ahmadi, *et al.*, "Demonstration of constant 8 W/mm power density at 10, 30, and 94 GHz in state-of-the-art millimeter-wave N-polar GaN MISHEMTs," *IEEE Trans. Electron Devices*, vol. 65, no. 1, pp. 45–50, 2018, doi: 10.1109/TED.2017.2770087.

[10] T. Lim, R. Aidam, P. Waltereit, T. Henkel, R. Quay, *et al.*, "GaN-based submicrometer HEMTs with lattice-matched InAlGaN barrier grown by MBE," *IEEE Electron Device Lett.*, vol. 31, no. 7, pp. 671–673, 2010, doi: 10.1109/LED.2010.2048996.

[11] G. H. Jessen, J. K. Gillespie, G. D. Via, A. Crespo, D. Langley, *et al.*, "RF power measurements of InAlN/GaN unstrained HEMTs on SiC substrates at 10 GHz," *IEEE Electron Device Lett.*, vol. 28, no. 5, pp. 354–356, 2007, doi: 10.1109/LED.2007.895417.

[12] A. Crespo, M. M. Bellot, K. D. Chabak, J. K. Gillespie, G. H. Jessen, *et al.*, "High-Power Ka-Band Performance of AlInN / GaN HEMT with 9.8-nm-Thin Barrier," *IEEE Electron Device Lett.*, vol. 31, no. 1, pp. 2009–2011, 2010.

[13] M. A. Caro, S. Zhang, T. Riekkinen, M. Ylilammi, M. A. Moram, *et al.*, "Piezoelectric coefficients and spontaneous polarization of ScAlN," *J. PHYSICS-CONDENSED MATTER*, vol. 27, no. 24, Jun. 2015, doi: 10.1088/0953-8984/27/24/245901.

[14] M. A. Moram and S. Zhang, "ScGaN and ScAlN: Emerging nitride materials," *J. Mater. Chem. A*, vol. 2, no. 17, pp. 6042–6050, 2014, doi: 10.1039/c3ta14189f.

[15] M. T. Hardy, B. P. Downey, N. Nepal, D. F. Storm, D. S. Katzer, and D. J. Meyer, "Epitaxial ScAlN grown by molecular beam epitaxy on GaN and SiC substrates," *Appl. Phys. Lett.*, vol. 110, no. 16, 2017, doi: 10.1063/1.4981807.

[16] T. E. Kazior, E. M. Chumbes, B. Schultz, J. Logan, D. J. Meyer, and M. T. Hardy, "High Power Density ScAlN-Based Heterostructure FETs for mm-Wave Applications," *IEEE MTT-S Int. Microw. Symp. Dig.*, vol. 2019-June, pp. 1136–1139, 2019, doi: 10.1109/mwsym.2019.8701055.

[17] J. Jungwoo and J. A. Del Alamo, "Critical Voltage for Electrical Degradation of GaN High-Electron Mobility Transistors," *Tech. Dig. - Int. Electron Devices Meet. IEDM*, vol. 29, no. 4, pp. 287–289, 2008, doi: 10.1109/IEDM.2006.346799.

[18] J. Kuzmik, G. Pozzovivo, C. Ostermaier, G. Strasser, D. Pogany, *et al.*, "Analysis of degradation mechanisms in lattice-matched InAlN/GaN high-electron-mobility transistors," *J. Appl. Phys.*, vol. 106, no. 12, 2009, doi: 10.1063/1.3272058.

[19] M. T. Hardy, B. P. Downey, D. J. Meyer, N. Nepal, D. F. Storm, and D. S. Katzer, "Epitaxial ScAlN etch-stop layers grown by molecular beam epitaxy for selective etching of AlN and GaN," *CS MANTECH 2017 - 2017 Int. Conf. Compd. Semicond. Manuf. Technol.*, vol. 30, no. 4, pp. 475–479, 2017.

[20] A. J. Green, J. K. Gillespie, R. C. Fitch, D. E. Walker, M. Lindquist, *et al.*, "ScAlN/GaN High-Electron-Mobility Transistors with 2.4-A/mm Current Density and 0.67-S/mm Transconductance," *IEEE Electron Device Lett.*, vol. 40, no. 7, pp. 1056–1059, 2019, doi: 10.1109/LED.2019.2915555.

[21] J. S. Moon, D. Wong, M. Hu, P. Hashimoto, M. Antcliffe, *et al.*, "55% PAE and high power Ka-band GaN HEMTs with linearized transconductance via n+ GaN source contact ledge," *IEEE Electron Device Lett.*, vol. 29, no. 8, pp. 834–837, 2008, doi: 10.1109/LED.2008.2000792.

[22] T. Palacios, A. Chakraborty, S. Rajan, C. Poblenz, S. Keller, and J. Speck, "High-power AlGaN/GaN HEMTs for Ka-band applications," *IEEE Electron Device Lett.*, vol. 26, no. 11, pp. 781–783, 2005, doi: 10.1109/LED.2005.857701.

[23] J. S. Moon, S. Wu, D. Wong, I. Milosavljevic, A. Conway, *et al.*, "Gate-Recessed AlGaN – GaN HEMTs for High-Performance Millimeter-Wave Applications," *IEEE Electron Device Lett.*, vol. 26, no. 6, pp. 348–350, 2005.

[24] M. Mi, X. H. Ma, L. Yang, Y. Lu, B. Hou, *et al.*, "Millimeter-Wave Power AlGaN/GaN HEMT Using Surface Plasma Treatment of Access Region," *IEEE Trans. Electron Devices*, vol. 64, no. 12, pp. 4875–4881, 2017, doi: 10.1109/TED.2017.2761766.

[25] R. C. Fitch, D. E. Walker, A. J. Green, S. E. Tetlak, J. K. Gillespie, *et al.*, "Implementation of High-Power-Density X-Band AlGaN/GaN High Electron Mobility Transistors in a Millimeter-Wave Monolithic Microwave Integrated Circuit Process," *IEEE Electron Device Lett.*, 2015, doi: 10.1109/LED.2015.2474265.

[26] M. A. Khan, G. Simin, J. Yang, J. Zhang, A. Koudymov, *et al.*, "Insulating gate III-N heterostructure field-effect transistors for high-power microwave and switching applications," *IEEE Trans. Microw. Theory Tech.*, vol. 51, no. 2 II, pp. 624–633, 2003, doi: 10.1109/TMTT.2002.807681.

[27] R. Chu, L. Shen, N. Fichtenbaum, Z. Chen, S. Keller, *et al.*, "Correlation between DC-RF dispersion and gate leakage in deeply recessed GaN/AlGaN/GaN HEMTs," *IEEE Electron Device Lett.*, vol. 29, no. 4, pp. 303–305, 2008, doi: 10.1109/LED.2008.917939.

[28] J. H. Davies, *The Physics of Low-dimensional Semiconductors: An Introduction*. Cambridge University Press, 1997.